ACS APPLIED MATERIALS & INTERFACES

Research Article

www.acsami.org

High Temperature Thermoelectric Properties of Strontium Titanate Thin Films with Oxygen Vacancy and Niobium Doping

S. R. Sarath Kumar, Abeer Z. Barasheed, and H. N. Alshareef*

Materials Science and Engineering, King Abdullah University of Science and Technology (KAUST), Thuwal-23955-6900, Saudi Arabia

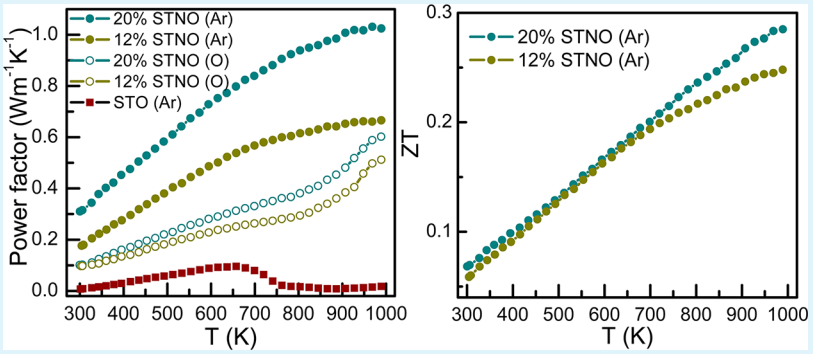

ABSTRACT: We report the evolution of high temperature thermoelectric properties of $SrTiO_3$ thin films doped with Nb and oxygen vacancies. Structure–property relations in this important thermoelectric oxide are elucidated and the variation of transport properties with dopant concentrations is discussed. Oxygen vacancies are incorporated during growth or annealing in Ar/H_2 above 800 K. An increase in lattice constant due to the inclusion of Nb and oxygen vacancies is found to result in an increase in carrier density and electrical conductivity with simultaneous decrease in carrier effective mass and Seebeck coefficient. The lattice thermal conductivity at 300 K is found to be 2.22 W m^{-1} K^{-1}, and the estimated figure of merit is 0.29 at 1000 K.

KEYWORDS: *thermoelectrics, oxide semiconductors, transport properties, pulsed laser deposition, oxygen vacancies*

1. INTRODUCTION

Thermoelectrics (TE) have received increased attention in recent years as one of the many potential technologies for sustainable energy production, in a world where severe energy crisis is in the looming. TE materials make use of the Seebeck and Peltier effects, respectively, for solid state power generation and refrigeration.[1,2] The ability of a TE material in converting energy from one form to another is expressed as a dimensionless figure of merit, $ZT = (S^2\sigma T/\kappa_e + \kappa_{ph})$, where S, σ, κ_e, and κ_{ph} are, respectively, the Seebeck coefficient, electrical conductivity, and electronic and lattice thermal conductivities.[3] For TE to compete with other technologies of energy conversion, a $ZT \geq 1$ is considered essential, while materials that satisfy this condition, especially at high temperatures, are scarce. Ceramic oxides are being investigated in this regard, since they are not only stable at high temperature and environmentally benign, but also economical.[4] Besides, the electrical properties of oxides can be tuned by doping with other elements or by creating vacancies, offering pathways to creating compounds with various chemical compositions in a quest for improving ZT.[5] While *p*-type oxides with a $ZT > 1$ are available, their *n*-type counterparts lag behind with the highest reported ZT of 0.37. A major challenge in the development of high ZT oxide TE is the inherently high κ_{ph} in oxides owing to the loosely held oxygen atoms which help in phonon conduction.[6] Efforts to minimize κ_{ph} only brought in only limited success.[6−8] It is hence important to tailor oxides for higher power factors (the numerator, $S^2\sigma T$, in the expression for ZT).

$SrTiO_3$ (STO) which is a cubic perovskite is a potential candidate for high temperature n-type oxide TE,[9] owing to the huge carrier effective mass.[10] STO is a wide band gap (3.2 eV) insulator[11] in its pristine form and can be made n-type by doping either the Sr with group III elements such as La,[12,13] Y,[14] and so forth, or the Ti sites with group V elements such as Nb,[13,15] Ta,[16] and so forth, or by creating oxygen vacancies.[11] However, substitutional doping is found to enhance carrier concentration only at the expense of Seebeck coefficient. Though the role of oxygen vacancies in enhancing carrier concentration of oxides is well established, the exact dynamics of oxygen vacancy creation in STO and Nb doped STO (STNO) and its effect on the Seebeck coefficient is less understood. While oxygen vacancies are reported to enhance the low temperature mobility of STO thin films[17] depending upon the thickness of the oxygen vacancy doped layer, the dependence of m^* on carrier density remains controversial. For instance, Okuda et al.[18] have reported an increase in m^* with carrier density for bulk La doped STO, while Ravichandran et

Received: May 1, 2013
Accepted: July 11, 2013
Published: July 11, 2013

   dx.doi.org/10.1021/am4015956 | ACS Appl. Mater. Interfaces 2013, 5, 7268−7273

al.[19] have reported on the contrary on oxygen deficient La doped STO films. Recently, we have reported[12] our findings on La doped STO films that matched with Okuda et al.'s findings. Though Ohta and co-workers[13,15] have reported the role of Nb dopant concentration on the TE properties of STNO single crystals and thin films, there are no experimental reports on the role of growth and annealing ambient in creating oxygen vacancies which determine the effective mass of STO and STNO films. Using density functional theory calculations, Wunderlich et al.[10] have tried to explain the complex dependence of effective mass on oxygen vacancies and carrier density in STO and other doped STO films. For smaller oxygen vacancy concentrations, the ab inito calculations predicted an increase in m^* while a decrease in m^* was predicted for high concentrations of oxygen vacancies. One of the reasons for ambiguity in the existing literature is the lack of sufficient care in choosing and reporting the ambient under which high temperature measurements are carried out. Oxides, though considered stable at high temperatures, are indeed prone to loss of oxygen or reoxidation, respectively, under reducing or oxidizing ambient at elevated temperatures and hence care must be taken in the conception and design of experiments and accurate reporting of the same.

In view of these issues, a comprehensive study on the role of oxygen vacancies and Nb dopants is undertaken in the present work. In order to understand the exact dependence of the transport and TE properties on Nb dopant and oxygen vacancy concentrations, STO and STNO films were grown in oxygen and Ar partial pressures, and the evolution of high temperature TE properties in Ar/H_2 is analyzed.

2. EXPERIMENTAL SECTION

STO and STNO films were deposited by PLD (Neocera, Beltsville, MD) using a KrF excimer laser (λ = 248 nm, pulse duration ~ 20 ns, repetition rate = 10 Hz). Films were deposited by ablation of 4N purity STO and STNO targets (Testbourne Ltd., England) at a laser fluence of 6 J cm^{-2} $pulse^{-1}$. The targets were held on a rotating carousel to ensure a uniform ablation from the target surface. Films were grown in 20 mTorr of oxygen, to maintain the oxygen stoichiometry of the target. For creating oxygen deficient films, 20 mTorr of Ar was introduced as a reducing gas, instead of oxygen, using a mass flow controller. Films were deposited on (100) oriented $LaAlO_3$ (LAO) substrates (MTI corporation), held at a temperature of 973 K using a rotating substrate holder which ensured uniform deposition.

The thickness of the films was measured using spectroscopic ellipsometry. The phase purity and orientation of the films were determined using θ–2θ (Bragg–Brentano) X-ray diffraction (XRD, D8 Bruker, AXS System, Germany) and by analyzing the XRD ϕ-scans. For the ϕ-scans, the (211) and (310) planes of STNO were selected. For (211) planes, the ϕ-scan was obtained by rotating the sample 360° around the surface normal, after tilting the sample by 35.26° and fixing 2θ at 57.796°, while the ϕ-scan of (310) plane was obtained after tilting the sample by 18.43° and fixing 2θ at 77.177°. The composition of the films was measured by high-resolution Rutherford backscattering spectrometry (HRBS-500, Kobelco, Japan), after depositing identical films with thickness less than 100 nm, on Si/SiO_2 substrates, since accurate measurement of composition of films on LAO substrates was difficult due to the high atomic number of La. For the HRBS studies, He^+ ion beam with energy 400 keV was used and the backscattered ions were collected at an angle of 169°. Simulations were performed using a custom-built code (Kobelco, Japan). The electrical conductivity and the Seebeck coefficient were measured in the range 300–1000 K by using respectively the linear four-probe and the differential methods, under Ar/H_2 (96% Ar and 4% H_2) ambient using a commercial setup (RZ2001i, Ozawa Science Co Ltd., Nagoya, Japan). Pt–Pt/Rh thermocouples were used as probes which simultaneously served the purpose of voltage and current probes as well as temperature sensors. Each measurement took ~20 h to complete. The automated setup allows simultaneous measurement of electrical conductivity and Seebeck coefficient at any given temperature, enabling studies on the evolution of the physical properties during annealing of the sample in the selected ambient. Cross-plane thermal conductivity of 20% STNO film grown in Argon was measured at 300 K by employing the 3ω method[20] (Fraunhofer IPM, Germany). Room temperature Hall effect measurements were carried out in a four-probe configuration using a physical property measurement system (PPMS, Quantum Design Inc.).

3. RESULTS AND DISCUSSION

The epitaxial growth on LAO substrate is evident from the XRD pattern of the films. Figure 1a shows the XRD pattern

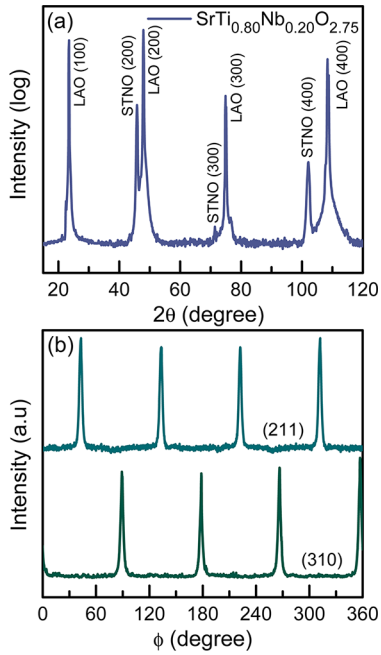

Figure 1. (a) θ–2θ XRD pattern for STNO films showing the epitaxial growth on (001) LAO substrate. (b) XRD ϕ scans for the (211) and (310) planes of the STNO film on (100) LAO substrate.

obtained for 20% STNO film. Similar spectra were obtained for the other films, albeit with finite shifts in the (200) peak position for the films. The calculated lattice constant of the films is shown in Table 1. As compared to undoped and stoichiometric STO, the lattice constants of the films are higher. For STO film grown in Ar, the increased lattice constant is due to oxygen vacancies. The absence of oxygen in the TiO_2 and SrO planes result in an increased electrostatic repulsion between the cations, resulting in the cations being displaced away from the oxygen vacancy, leading to an expansion of the unit cell. For STNO films, the lattice constant increases with both oxygen vacancies and Nb concentration. In STNO films, larger Nb^{5+} ions (ionic radius = 0.780 Å) substitute for the smaller Ti^{4+} ions (ionic radius = 0.745 Å) in an octahedral coordination, resulting in the expansion of the lattice. The increase in lattice constant plays a significant role in determining the Seebeck coefficient of the films and will be discussed later. The epitaxial growth is confirmed from the ϕ scan measurements on the films (shown in Figure 1b). The ϕ scan pattern for the (211) and (310) planes of the film reveals

dx.doi.org/10.1021/am4015956 | ACS Appl. Mater. Interfaces 2013, 5, 7268–7273

Table 1. Lattice Constant Together with the Transport and Thermoelectric Properties of STO and STNO Films at 300 K[a]

film	Nb conc/ ambient	lattice constant (Å)	carrier concentration ($\times 10^{21}$ cm^{-3})	Hall mobility (cm^2 V^{-1} s^{-1})	m^*/m_0			electrical conductivity (S cm^{-1})	Seebeck coefficient (μV K^{-1})
					$r = 0$	$r = 2$	$r = 1$		
$SrTi_{0.80}Nb_{0.20}O_{2.75}$	20%/Ar	3.968	1.32	15.6	1.98	0.66	0.99	3294.7	−56
$SrTi_{0.88}Nb_{0.12}O_{2.75}$	12%/Ar	3.952	1.01	7.3	2.10	0.70	1.05	1182.3	−70
$SrTi_{0.80}Nb_{0.20}O_3$	20%/O_2	3.962	0.92	3.1	2.68	0.89	1.34	453.0	−86
$SrTi_{0.88}Nb_{0.12}O_3$	12%/O_2	3.949	0.83	1.4	3.16	1.05	1.58	188.2	−131
$SrTiO_{2.75}$	0%/Ar	3.928	0.05	0.3				2.2	−338

[a]The carrier effective mass with respect to the free electron mass (m^*/m_0) for different scattering parameters (r) is also shown. The values 0, 2, and 1 for r correspond to acoustic phonon scattering, ionized impurity scattering, and mixed scattering, respectively.

the 4-fold symmetry axis normal to the surface. The shift in the peak positions is exactly 45°, clearly demonstrating that the films are grown epitaxial on (100) LAO substrates. The full width at half-maximum of the peaks is small (2.2°), indicating that the crystallites are well aligned resulting in a high quality cube-on-cube epitaxial relation. The thickness of the films is 300 ± 10 nm. The grain size (~1500 nm), as estimated using Scherrer formula, is much larger than the thickness, confirming the in-plane growth of the films. No change in grain size was observed before and after subjecting the films to thermoelectric measurements, suggesting that microstructural changes, that can affect the transport properties, are negligible. It is hardly surprising to note that the high temperature measurements have no effect on the microstructure, since the films were grown at 973 K, while the thermoelectric measurements were done up to nearly the same temperature (1000 K).

The composition of the films was estimated using HRBS, and the typical HRBS spectra of 12% STNO grown in Ar on Si/SiO_2 substrate is shown in Figure 2. The high energy edge

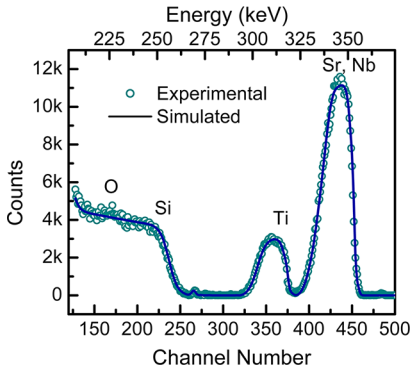

Figure 2. HRBS spectra of STNO film on Si/SiO_2 substrate, grown under identical conditions as on (001) LAO substrate. The symbols correspond to the experimental, and the line corresponds to the simulated data. The edges corresponding to the elements of the film and the substrate are marked.

corresponds to the high atomic number elements (Sr and Nb). Since the atomic numbers are close (38 and 41, respectively), Sr and Nb offer similar cross sections for scattering of the ion beam and hence the backscattered signals overlap. Ti shows up at intermediate energies while oxygen from the film and the substrate appears as superimposed peaks on the Si plateau, resulting from the thickness of the Si substrate. The compositional analysis shows that the film is better represented as $Sr(Ti_{0.88},Nb_{0.12})O_{3-\delta}$, where $\delta = 0.25$ represents the amount of oxygen vacancies per formula unit. While the cationic compositions are precise within 1%, the error in oxygen composition is around 5%, due to the poor yield of RBS on elements with low atomic numbers. It may be noted that STO preserves the cubic perovskite structure even for δ as high as 0.5.[11] The 20% STNO film grown in Ar is better represented as $SrTi_{0.80}Nb_{0.20}O_{3-\delta}$, with δ being 0.25, while δ is negligibly small (within the error) for films grown in oxygen.

The electrical conductivity of the films as a function of temperature is shown in Figure 3. Nb doped films show a

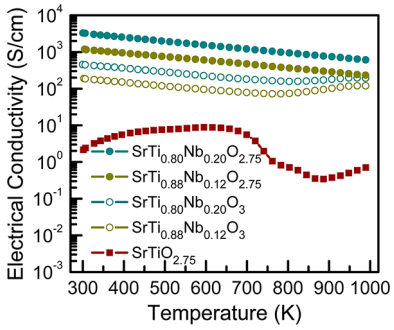

Figure 3. High temperature electrical conductivity of STO and STNO films, measured in Ar/H_2 ambient. The solid symbols correspond to films grown in Ar, while the open symbols correspond to films grown in oxygen.

degenerate behavior in the entire temperature range, irrespective of the ambient under which they are grown. The electrical conductivity at any temperature is found to increase with Nb concentration. Clearly, Nb^{5+} ions act as donors, since they substitute for Ti^{4+} in the lattice, driving the density of carriers above the critical density for metallic conduction. Increase in Nb concentration results in more carriers and hence higher conductivity. Also, films grown in Ar (solid symbols) show a higher conductivity than the corresponding films grown in oxygen, pointing to the role of oxygen vacancies. Growth in oxygen ambient results in STO films with less oxygen vacancies and hence, low carrier density and low conductivity, as evident from Table 1. On the other hand, growth in Ar favors the creation of oxygen vacancies, which form a donor band close to the conduction band edge. With each of the vacancies donating two electrons to the conduction band, the carrier density increases, resulting in enhanced conductivity. An interesting feature observed in STNO films grown under oxygen is a change in slope around 800 K followed by an increase in conductivity. This is attributed to the creation of oxygen vacancies during TE measurements in the reducing Ar/H_2 ambient. For these films, the data obtained while cooling (Figure 4a) show a higher conductivity compared to that obtained during heating, suggesting that the films underwent an

dx.doi.org/10.1021/am4015956 | ACS Appl. Mater. Interfaces 2013, 5, 7268−7273

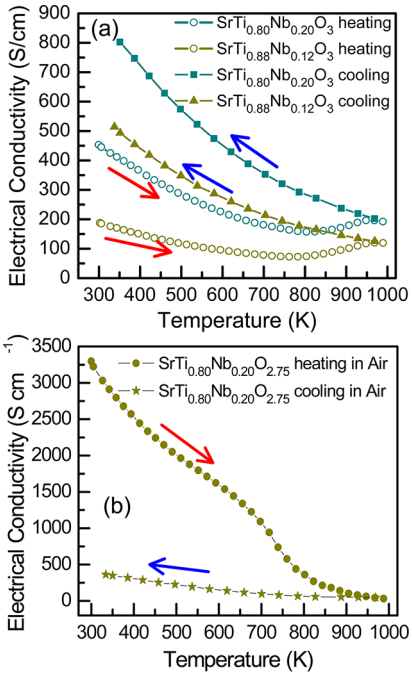

Figure 4. (a) Difference in heating and cooling curves in Ar/H_2, in the high temperature electrical conductivity of STNO films grown in oxygen. The hysteresis is due to the irreversible changes caused by the loss of oxygen beyond 800 K. (b) Difference in the high temperature electrical conductivity of 20% STNO film grown in Ar, for measurements done in air. The hysteresis is due to irreversible changes brought in by refilling of the oxygen vacancies. The red and blue arrows represent heating and cooling, respectively.

irreversible change during the measurement beyond 800 K. The magnitude of the hysteresis reduced drastically in the next cycle of measurement (not shown). A similar hysteresis, but with a decrease in conductivity during cooling, is observed (Figure 4b) when measured in air, for STNO films grown in Ar. The observed changes can be accounted for if one considers the refilling of oxygen vacancies, when heated in air. Even though the most probable operation ambient for practical purposes is air, due to the detrimental decrease in conductivity which in turn resulted in a reduced power factor during high temperature measurement in air, further studies were done in Ar/H_2 ambient. Interestingly, the data obtained during heating and cooling for the STNO films grown under Ar (not shown) exhibited no such hysteresis when measured in Ar/H_2, indicating that sufficient number of oxygen vacancies is created during the growth itself. This is hardly surprising since the high temperature (973 K) growth of the films in the inert Ar partial pressure ensures perfect conditions for the creation of vacancies resulting in an equilibrium oxygen vacancy concentration, for subsequent heating, in a predominantly Ar gas mixture, up to comparable temperatures (1000 K, for our measurements). However, for the undoped STO films, an equilibrium oxygen vacancy is not established for subsequent anneals as evident from the changes in the curve with annealing. The undoped STO film grown in oxygen was too resistive to be measured using the four-probe method, which is attributed to the fact that stoichiometric STO is a perfect wide band gap insulator. The one grown in Ar, however, exhibits measurable conductivity (Figure 3), which increases with temperature, below ~650 K, which is characteristic of semiconductors. In the range 650–850 K, there is a fall in electrical conductivity, with a subsequent increase beyond 900 K. The fall in conductivity is opposite to the trend shown by STNO films and is attributed to an order of magnitude lower carrier density and drastically lower mobility of STO compared to the STNO films.

The high temperature Seebeck coefficient of the films is shown as inset to Figure 5. A typical n-type behavior is

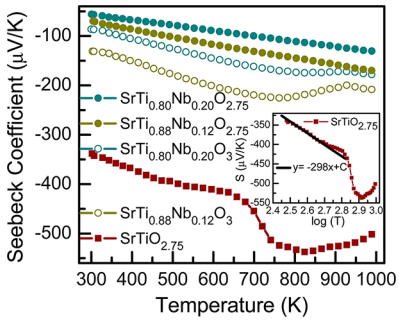

Figure 5. Seebeck coefficient of STO and STNO films as a function of temperature. The solid symbols correspond to films grown in Ar, while the open symbols correspond to films grown in oxygen. Inset shows the plot of Seebeck coefficient of STO film grown in Ar with $\log(T)$. The straight line shows the linear fit with a slope of -298 μV K^{-1} decade^{-1}, indicative of nondegenerate conduction.

observed, as evident from the sign of the Seebeck coefficient. STNO films grown in Ar (solid symbols) that showed typical degenerate semiconducting behavior exhibited a linear increase of absolute Seebeck coefficient with temperature. No Heikes limit was observed in the temperature range of interest. For the STNO films grown in oxygen, a decrease in absolute Seebeck coefficient occurs at ~800 K, the same temperature at which the electrical conductivity of the films changed. Similarly, for STO film grown in Ar, the changes in the curvature of the Seebeck coefficient curve coincide with the changes in the electrical conductivity of that film with temperature and hence are attributed to a common origin. The nondegenerate conduction evident from the electrical conductivity curve for STO film grown in Ar (Figure 3) manifests itself in the Seebeck coefficient curve as evident from the inset to Figure 5, where the Seebeck coefficient of STO film grown in Ar is plotted as a function of $\log(T)$. The low temperature data below the advent of oxygen vacancy creation could be fitted with a line of slope -298 μV K^{-1} decade^{-1}, expected for nondegenerate conduction as per the relation, $S \propto (-3K_B/2e)\ln(T)$. A strong dependence of Seebeck coefficient on the mobility of the films is evident from Table 1; films with higher mobility have lower values of absolute Seebeck coefficient. For the degenerate STNO films, this dependence can be understood considering how Seebeck coefficient depends on the effective mass, through the relation, $S_T = [(8\pi^{8/3}k_B^2 m^* n^{-2/3})/(3^{5/3}h^2 e)](r+1)T$, when a time independent mean free path and parabolic bands are assumed. In the relation mentioned above, m^* is the effective mass of electrons, n is the carrier density, k_B is the Boltzmann constant, h is the Planck's constant, e is the electronic charge, and r is the scattering parameter which varies with the scattering mechanism under consideration. The effective mass of the carriers around 300 K can be estimated from the slopes of the linear part of the $S-T$ curves of the films, assuming different scattering processes. The values obtained for $r = 0$ (acoustic phonon scattering, valid at temperatures much above the Debye temperature of STO, 513 K),[21] $r = 2$ (ionized impurity scattering, valid much below the Debye temperature),

dx.doi.org/10.1021/am4015956 | ACS Appl. Mater. Interfaces 2013, 5, 7268–7273

and $r = 1$ (mixed scattering, valid at temperatures around the Debye temperature) is shown in Table 1. In the absence of any high temperature Hall effect data, it is difficult to comment further on the specific scattering processes involved in different regimes of temperature. However, an increase in effective mass with decrease in carrier density is evident (Figure 6). While this

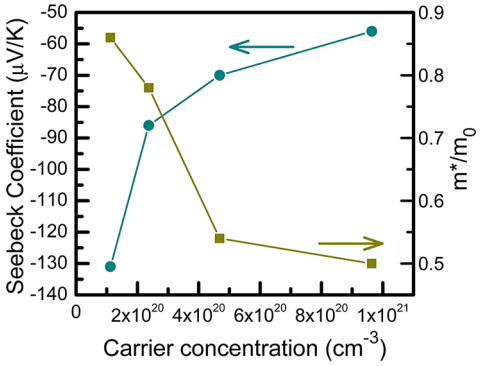

Figure 6. Dependence of Seebeck coefficient and carrier effective mass on carrier density of the films.

dependence is in agreement with the low temperature results of Ravichandran et al.[19] and the theoretical predictions of Wunderlich et al.,[10] it is in variance with low temperature single crystal data of Okuda et al.[18] and our previous report on high temperature TE properties of La doped STO films.[12] In order to resolve this contradiction, it is important to consider the oxygen vacancy concentration and the lattice constant of the films. On one hand, the single crystals grown by Okuda et al. were near stoichiometric with negligible oxygen vacancies. The lattice constant of the LSTO films previously reported by our group is in the range 3.906−3.911 Å, which also stems from low La and oxygen vacancy concentrations. On the other hand, the La doped STO films grown by Ravichandran et al. were significantly reduced with lattice constants as high as 4.075 Å. In the present studies, the STNO films have similar high lattice constants, especially the ones grown in Ar, which are heavily reduced. In STNO films, the bottom of conduction band is predominantly made of Ti 3d orbitals and an increase in lattice constant implies enhanced orbital overlapping between adjacent Ti ions. In other words, the oxygen vacancies and higher Nb concentration induce a tetragonal distortion of the Ti sublattice, effectively lifting the 6-fold degeneracy of the conduction band to a 4-fold one, leading to a higher band curvature and hence, a lower m^*.[10] As evident from Table 1, m^* indeed decreases with an increase in lattice constant and carrier density and the dependence of Seebeck coefficient of STNO films (Figure 6) on the effective mass can be better understood by considering the direct correlation of m^* with lattice constant. For oxygen rich STO and doped STO films, the tetragonal distortion can be neglected and hence m^* increases with carrier density as previously reported.

It is noticeable that a comparison of Figures 3 and 5 reveals the inverse trends for absolute Seebeck coefficient and electrical conductivity, which is generally true for TE materials. Hence, these physical quantities need to be optimized for an enhanced power factor (taken as $S^2\sigma T$, in units of W m^{-1} K^{-1}). The power factor as a function of temperature is shown in Figure 7. The 20% STNO film grown in Ar shows the best power factor among the films studied, despite the low Seebeck coefficient, owing to its superior electrical conductivity. From the lower

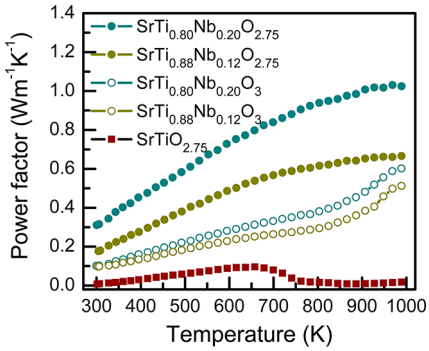

Figure 7. Thermoelectric power factor (in W m^{-1} K^{-1}) of STO and STNO films as a function of temperature.

values of power factor for STO film grown in Ar, it is evident that enhancement of electrical conductivity is crucial for developing STO based TE.

The total cross-plane thermal conductivity, κ, of 12% STNO film grown in Ar is found to be 3.1 W m^{-1} K^{-1}, at 300 K, employing the 3ω method. The error in the measurement is typically within 5%. Since STO is cubic, it is reasonable to expect that thermal conductivity is isotropic and hence in-plane value is assumed to be same as the cross-plane one. Using the Wiedemann−Franz relation $\kappa_e = L_0\sigma T$, where L_0 is the Lorentz number (taken as 2.45 × 10^{-8} W Ω K^{-2} for $SrTiO_3$), and the relation $\kappa = \kappa_{ph} + \kappa_e$, the lattice thermal conductivity at 300 K is estimated to be 2.22 W m^{-1} K^{-1}, which is slightly lower compared to the reported 3 W m^{-1} K^{-1} for undoped single crystalline STO bulk. The lower value may be due to the oxygen vacancies in the film which scatter the phonons.[6] Lattice thermal conductivity of crystalline films usually decreases at temperatures above the Debye temperature, and hence, a higher estimate of the total thermal conductivity at high temperatures can be extracted by applying the electrical conductivity values to the Weidemann−Franz relation and using the room temperature value of κ_{ph}. Assuming that κ_{ph} is independent of Nb concentration,[15] ZT of STNO films grown in Ar is then estimated and plotted in Figure 8. A ZT value of

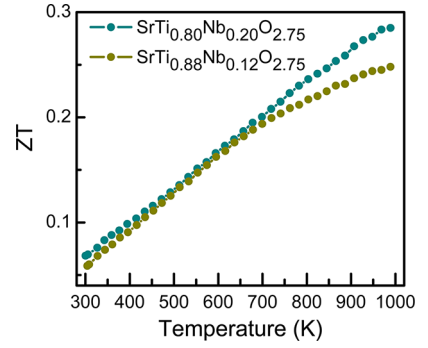

Figure 8. Estimated high temperature ZT of STNO films grown in Ar.

0.29 is obtained for 20% STNO film and compares well with that previously reported,[15] though their individual values of Seebeck coefficient and electrical conductivity are quite different, owing to different growth conditions. The identical values of ZT obtained even after following different deposition conditions suggest that tunability of electrical properties is possible without affecting ZT and the value 0.29 is close to the upper limit possible in STNO films. Hence, potential routes to

enhance ZT in STO based films must focus on enhancing the power factor by doping for both Sr and Ti, which will also help reduce the lattice thermal conductivity due to possible mass-fluctuation scattering and also on creation of artificial superlattices and mesostructures with a view to attack wider phonon spectra.

4. CONCLUSIONS

In summary, we have grown epitaxial thin films of undoped and doped STO, with different Nb concentrations and oxygen vacancies, on LAO substrates and the high temperature evolution of thermoelectric properties was analyzed. While films grown in Ar showed reproducible heating and cooling curves for electrical conductivity and Seebeck coefficient, the ones grown in oxygen showed irreversible changes which are attributed to the creation of additional oxygen vacancies above 800 K. The lattice constant of STNO was found to increase with both Nb and oxygen vacancy concentrations and a direct dependence of lattice constant with the transport properties was observed. The carrier density and electrical conductivity were found to increase while the effective mass and Seebeck coefficient were found to decrease with an increase in lattice constant, brought in by the tetragonal distortion of the lattice. Tuning of effective mass and hence the thermoelectric properties is possible in this technologically important TE material, and a high ZT value of 0.29 at 1000 K is estimated.

AUTHOR INFORMATION

Corresponding Author

*E-mail: husam.alshareef@kaust.edu.sa.

Notes

The authors declare no competing financial interest.

ACKNOWLEDGMENTS

This work was supported by the FIC grant of KAUST, for oxide thermoelectrics. Authors also thank Dr. Alexandre Jacquot, Fraunhofer IPM, Germany for the thermal conductivity measurements.

REFERENCES

(1) Tritt, T. M.; Subramanian, M. A. *MRS Bull.* **2006**, *31*, 188−194.
(2) Uher, C. *Semiconductors and Semimetals*; Academic Press: New York, 2001; Vol. *69*.
(3) Rowe, D. M. *Thermoelectrics Handbook: Macro to Nano*; CRC Press/Taylor and Francis: Boca Raton, FL, 2006.
(4) Zhang, R.-z.; Hu, X.-y.; Guo, P.; Wang, C.-l. *Phys. B* **2012**, *407*, 1114−1118.
(5) Koumoto, K.; Wang, Y.; Zhang, R.; Kosuga, A.; Funahashi, R. *Annu. Rev. Mater. Res.* **2010**, *40*, 363−394.
(6) Yu, C.; Scullin, M. L.; Huijben, M.; Ramesh, R.; Majumdar, A. *Appl. Phys. Lett.* **2008**, *92*, 191911.
(7) Wang, N.; He, H. C.; Ba, Y. S.; Wan, C. L.; Koumoto, K. *J. Ceram. Soc. Jpn.* **2010**, *118*, 1098−1101.
(8) Wang, N.; He, H. C.; Li, X. A.; Han, L.; Zhang, C. Q. *J. Alloys Compd.* **2010**, *506*, 293−296.
(9) Ohta, H. *Mater. Today* **2007**, *10*, 44−49.
(10) Wunderlich, W.; Ohta, H.; Koumoto, K. *Phys. B* **2009**, *404*, 2202−2212.
(11) Perez-Casero, R.; Perrière, J.; Gutierrez-Llorente, A.; Defourneau, D.; Millon, E.; Seiler, W.; Soriano, L. *Phys. Rev. B* **2007**, *75*, 165317.
(12) Kumar, S. R. S.; Abutaha, A. I.; Hedhili, M. N.; Alshareef, H. N. *J. Appl. Phys.* **2012**, *112*, 114104.
(13) Ohta, S.; Nomura, T.; Ohta, H.; Koumoto, K. *J. Appl. Phys.* **2005**, *97*, 034106.
(14) Ito, M.; Matsuda, T. *J. Alloys Compd.* **2009**, *477*, 473−477.
(15) Ohta, S.; Nomura, T.; Ohta, H.; Hirano, M.; Hosono, H.; Koumoto, K. *Appl. Phys. Lett.* **2005**, *87*, 092108.
(16) Cui, Y.; Salvador, J.; Yang, J.; Wang, H.; Amow, G.; Kleinke, H. *J. Electron. Mater.* **2009**, *38*, 1002−1007.
(17) Kozuka, Y.; Kim, M.; Ohta, H.; Hikita, Y.; Bell, C.; Hwang, H. Y. *Appl. Phys. Lett.* **2010**, *97*, 222115.
(18) Okuda, T.; Nakanishi, K.; Miyasaka, S.; Tokura, Y. *Phys. Rev. B* **2001**, *63*, 113104.
(19) Ravichandran, J.; Siemons, W.; Scullin, M. L.; Mukerjee, S.; Huijben, M.; Moore, J. E.; Majumdar, A.; Ramesh, R. *Phys. Rev. B* **2011**, *83*, 035101.
(20) Cahill, D. G. *Rev. Sci. Instrum.* **1990**, *61*, 802−808.
(21) Ahrens, M.; Merkle, R.; Rahmati, B.; Maier, J. *Phys. B* **2007**, *393*, 239−248.